RSC Advances

ROYAL SOCIETY OF CHEMISTRY

www.rsc.org/advances

Journal Name

ARTICLE

Three Metal Complexes Derived from 3-Methyl-1*H*-Pyrazole-4-Carboxylic Acid: Synthesis, Crystal Structures, Luminescence and Electrocatalytic Properties

Received 00th January 20xx,
Accepted 00th January 20xx

DOI: 10.1039/x0xx00000x

www.rsc.org/

Jing Liu[a, b], Mei-Ling Cheng[a], Li-Li Yu [a], Sheng-Chun Chen[a], Yong-Liang Shao[c], Qi Liu*[a, d], Chang-Wei Zhai[a] and Feng-Xiang Yin*[b]

Mononuclear complexes $[Cd(HMPCA)_2(H_2O)_4]$ (**1**) and $[Co(H_2MPCA)_2(DMF)_2(H_2O)_2]Cl_2$ (**2**), and 3D coordination polymer $[Cd_3Cl_2(HMPCA)_4(H_2O)_2]\cdot 2H_2O$ (**3**) (H_2MPCA = 3-methyl-1*H*-pyrazole-4-carboxylic acid) were synthesized and characterized by elemental analysis, IR spectra, thermogravimetric analysis, and X-ray single-crystal structure analysis. In **3**, $HMPCA^-$ anions bridged trinuclear Cd (II) ions clusters to form an 8-connected 3D network with channels. The complexes all display grenn fluorescence in the solid state. As a bifunctional catalyst, complex **2** exhibited excellent catalytic activity for oxygen evolution reaction (OER), and certain catalytic activity for oxygen reduction reaction (ORR).

.

Introduction

Construction of novel supramolecular frameworks and coordination polymers, especially their porous congeners, which are frequently termed metal-organic frameworks (MOFs), has become a promising field, not only owing to their intriguing structural features, but also due to their potential applications in magnetic and optical materials, catalysis, gas storage and separation and energy storage.[1-8] Organic ligands play a key role in assembling coordination polymers. Aza-cyclic carboxylic acids ligands as good building blocks in the design of MOFs are receiving increasing attention,[9-14] owing to their rich coordination modes. Pyrazole-carboxylic acids, such as 1*H*-pyrazole-4-carboxylic acid, 3,5-pyrazoledicarboxylic acid, 3,5-dimethyl-1*H*-pyrazole-4-carboxylic acid and 3-phenyl-1*H*-pyrazole-4-carboxylic acid etc, have been used to synthesize various MOFs with specific topologies and outstanding properties.[15-24] Recent years, we have also designed and synthesized many metal complexes using pyrazole-carboxylic acids ligands,[25-27] including 3,4-pyrazoledicarboxylic acid, 5-methyl-1*H*-pyrazole-3-carboxylic acid, and 1-carboxymethyl-5-methyl-1*H*-pyrazole-4-carboxylic acid etc. However, to the best of our knowledge, there have been no reports of metal complexes based on 3-methyl-1*H*-pyrazole-4-carboxylic acid (H_2MPCA) so far.

During the past few years, considerable attention has been paid to rechargeable aqueous lithium–air batteries due to their extremely high theoretical specific energy and the solubility of discharge product in water.[28, 29] However, the sluggish kinetics for oxygen reduction reaction (ORR) and oxygen evolution reaction (OER) can result in the decreasing of round-trip efficiency and cycle life of the lithium–air batteries.[30] Therefore, it is vital to develop an effective bifunctional electrocatalyst for both ORR and OER. To this end, some kinds of electrocatalysts such as PtAu/C, [31] and mesoporous α-MnO_2/Pd [32] nanocomposites have been demonstrated as catalysts for ORR and OER. Nevertheless, the high cost and scarcity of the noble metals hamper further development of rechargeable lithium–air batteries based on these materials. Therefore, considerable effort has been expended to develop non-noble bifunctional catalysts for practical use,[33-36] such as Co_3O_4/N-doped graphene, [33] and $NiCo_2O_4$ nanoflakes.[36]

On the other hand, metal complexes of phthalocyanine, porphyrin, Schiff base, aza-cyclic compounds and their derivatives, as a type of non-noble materials, have been widely used in the field of electrocatalysis owing to the devisable catalytic sites and fully available active center, which made it possible to catalyze ORR as electrocatalyst in the fuel cell and lithium–air batteries.[37-39] Recently, MOFs, as electrocatalysts

[a] School of Petrochemical Engineering and Jiangsu Key Laboratory of Advanced Catalytic Materials and Technology, Changzhou University, 1 Gehu Road, Changzhou, Jiangsu 213164, P. R. China. E-mail: liuqi62@163.com.
[b] Changzhou Institute of Advanced Materials, Beijing University of Chemical Technology, Changzhou, 213164, P. R. China.yinfix@mail.buct.edu.cn
[c] Department of Chemistry, Lanzhou University, Lanzhou, 730000, P. R. China
[d] State Key Laboratory of Coordination Chemistry, Nanjing University, Nanjing, Jiangsu 210093, China.

Electronic Supplementary Information (ESI) available: IR spectra, TGA curves, selected bond distances and angles for compounds **1-3,** electrode transfer number for ORR using complex **2**, OER stabilty test of complex **2**. CCDC Nos. 977149, 1003672, 1003671 are for **1**–**3**, respectively. *For ESI and crystallographic data in CIF or other electronic formatSee DOI: 10.1039/x0xx00000x*

for ORR, have been reported.[40] However, to the best of our knowledge, up to now, multi-functional electrocatalysts based on metal complexes have been less explored. Recently, K. P. Loh group prepared graphene oxide (GO)-incorporated Cu-MOF composite and found that it shows good performance as a tri-functional catalyst in three important electrocatalysis reactions, namely: the hydrogen evolution reaction (HER), OER and ORR.[41] Considering Co complexes have been used as electrocatalysts of ORR,[39] it is worth to investgate the bi-functional electrocatalytic activity of Co complexes for ORR and OER. Herein, we report the synthesis, crystal structures, and luminescent properties of three novel metal complexes $[Cd(HMPCA)_2(H_2O)_4]$ (**1**), $[Co(H_2MPCA)_2(DMF)_2(H_2O)_2]Cl_2$ (**2**) and $[Cd_3Cl_2(HMPCA)_4(H_2O)_2]\cdot 2H_2O$ (**3**) and the bi-functional electrocatalytic activity of complex **2** for ORR and OER.

Experimental Section

Materials and Characterization

All commercially available solvents and reagents were used as received without further purification unless otherwise noted. The ligand H_2MPCA was prepared according to the literature.[42] Elemental analysis (C, H and N) was performed on a Perkin-Elmer 2400 Series II element analyzer. FTIR spectra were recorded on a Nicolet 460 spectrophotometer in the form of KBr pellets. The luminescent spectra of the solid samples were recorded on a Varian Cary Eclipse spectrometer. Thermogravimetric analysis (TGA) experiments were carried out on a Dupont thermal analyzer from room temperature to 800 °C under N_2 atmosphere at a heating rate of 10°C·min^{-1}. Single-crystal X-ray diffraction measurement of the complexes **1**, **2** and **3** were carried out with a Bruker Apex II CCD diffractometer.

Synthesis

Preparation of $[Cd(HMPCA)_2(H_2O)_4]$ (**1**): A solution of H_2MPCA (0.0252 g, 0.20 mmol) and imidazole (0.0272 g, 0.40 mmol) in EtOH (2 mL) was added a solution of $CdCl_2\cdot 2.5H_2O$ (0.0457 g, 0.20 mmol) in 2 mL H_2O at room temperature, and the resulting solution was heated at 60 °C for 12 h, then filtered. The filtrate was allowed to stand at ambient temperature for 1 month to afford light yellow needlelike crystals **1** ($[Cd(HMPCA)_2(H_2O)_4]$) (41% yield based on Cd). Anal. Calcd for **1** (%): C, 28.02; H, 2.82; N, 13.07. Found: C, 28.01; H, 2.79; N, 13.05. IR data (cm^{-1}, KBr pellet): 3446 (m), 3237 (m), 1630(m), 1537 (s), 1488 (m), 1436 (s), 1325 (s), 1062 (s), 844 (m), 744 (s) 647 (s), 610 (s).

Preparation of $[Co(H_2MPCA)_2(DMF)_2(H_2O)_2]Cl_2$ (**2**): A solution of H_2MPCA (0.0252 g, 0.20 mmol) and NaOH (0.0080 g, 0.20 mmol) in MeOH and DMF (2 mL, v:v=1:1) was added a solution of $CoCl_2\cdot 6H_2O$ (0.0237 g, 0.10 mmol) in 2 mL H_2O under oscillation by the ultrasonic-wave reactor (100 W). When much precipitate produced, 1 mol/L HCl solution was added until the solution became clear. The resulting solution was filtered, and the filtrate was allowed to stand at ambient temperature for 2 months to afford red crystals **2** ($[Co(H_2MPCA)_2(DMF)_2(H_2O)_2]Cl_2$) (50% yield based on Co). Anal. Calcd for **2**, (%): C, 34.18; H, 5.02; N, 14.95. Found: C, 34.15; H, 5.01; N, 14.92. IR data (cm^{-1}, KBr pellet): 3439 (m), 3347(s), 3254 (s), 3104 (s), 1685 (s), 1634(m), 1524 (s), 1452(m), 1410(m), 1219 (s), 1141 (s), 795 (m), 717 (m).

Preparation of $[Cd_3Cl_2(HMPCA)_4(H_2O)_2]\cdot 2H_2O$ (**3**): A solution of H_2MPCA (0.0252 g, 0.20 mmol) in DMF (1 mL) was added a solution of $CdCl_2\cdot 2.5H_2O$ (0.0457 g, 0.20 mmol) in MeOH (1 mL) and H_2O (1 mL) at room temperature. After 2 h, a solution of 2,2'-bipyridine (2,2'-bipy) (0.0156 g, 0.10 mmol) in 2 mL MeOH was added, resulting in the solution becoming turbid. The resulting mixture was heated at 60 °C for 22 h, then filtered, and the filtrate was allowed to stand at ambient temperature for 1 month to afford colorless rhombus crystals **3** ($[Cd_3Cl_2(HMPCA)_4\cdot(H_2O)_2]\cdot 2H_2O$) (44% yield based on Cd). Anal. Calcd for **3** (%): C, 24.49; H, 2.88; N, 11.43. Found: C, 24.38; H, 2.79; N, 11.37. IR data (cm^{-1}, KBr pellet): 3451 (m), 3346 (s), 3275 (s), 1700(s), 1575 (s), 1518 (s), 1461 (m), 1281 (s), 1131 (m), 1098 (m), 958 (s), 780 (m), 701 (m), 681 (m).

X-ray Crystallography

Single-crystal X-ray diffraction measurements of **1**, **2** and **3** were carried out with a Bruker Smart Apex CCD diffractometer at 293 (2) K, 296 (2) K and 296 (2) K respectively. Intensities of reflections were measured using graphite-monochromatic Mo-Kα radiation (λ = 0.7107 Å) with the ψ-ω scans mode from $2.85^\circ < \vartheta < 28.02^\circ$ (**1**) $2.50^\circ < \vartheta < 27.11^\circ$ (**2**) and $2.22^\circ < \vartheta < 27.65$ (**3**). The structure was solved by direct methods using Olex 2 for **1** and **3**, SHELXTL-97 for **2**, they are all refined by full-matrix least-squares on F^2 with the SHELXTL-97 program package.[43, 44]

Table 1. Crystal Structure Parameters of 1-3

Complex	1	2	3
Empirical formula	$C_{10}H_{18}CdN_4O_8$	$C_{16}H_{30}CoN_6O_8Cl_2$	$C_{20}H_{28}Cd_3Cl_2N_8O_{12}$
Formula weight	434.68	564.29	980.60
Crystal size (mm)	0.32×0.27×0.25	0.28×0.27×0.25	0.26×0.22×0.20
Crystal system	Triclinic	Monoclinic	Monoclinic
T (K)	293(2)	296(2)	296(2)
Space group	$P\bar{1}$	$P2_1/c$	$P2_1/n$
a (Å)	7.2694 (10)	8.2310 (4)	9.5870 (2)
b (Å)	7.2818 (11)	16.953 (8)	14.232 (3)
c (Å)	8.2989 (12)	9.447 (4)	12.454 (3)
α (°)	111.267	90.000	90.000
β (°)	109.883	99.817	104.76 (5)
γ (°)	91.968	90.000	90.000
V (Å^3), Z	378.69 (5), 1	1299.0(5), 2	1643.1 (6), 2
R_{int}	0.0230	0.0829	0.0700
Calculated density (g·cm^{-3})	1.906	1.433	1.982
μ (mm^{-1})	1.491	0.916	2.153
F(000)	218	586	956
θ range for data collection (°)	2.85 - 28.02	2.50 - 27.11	2.22 - 27.65
Index ranges (h, k, l)	-8/8,-8/8,-10/7	-10/10,-12/20,-11/11	-12/12,-18/17,-11/15
Independent reflections (R_{int})	1369	2547	3655
Refinement method	full-matrix least-squares on F^2		
Data/restraints/ parameters	1369 / 9 / 116	2547 / 1 / 158	3665 / 3 / 208
Goodness-of-fit on F^2	1.061	1.061	1.045
R_1, wR_2 [I>2σ(I)]	0.0366, 0.0977	0.0681, 0.1815	0.0548, 0.1279
R_1, wR_2(all data)	0.0371, 0.0982	0.1019, 0.2273	0.0832, 0.1377
Largest difference peak and hole (e·Å^{-3})	1.13 and -0.67	0.72 and -0.72	1.18 and -1.12

Anisotropic thermal factors were assigned to all the non-hydrogen atoms. Hydrogen atoms were included in calculated parameters riding on the parent atoms. H atoms bonded to O or N were first located in difference Fourier maps and then placed in positions and refined with isotropic thermal calculated sites and included in the refinement. Crystallographic data and experimental details for structural analyses are summarized in Table 1.

Electrochemical Measurement

The working electrode was prepared with complex **2** as catalyst as follows: 2.5 mg of complex **2** and 2.5 mg of carbon black (Vulcan XC-72) were mixed in 1 mL EtOH and 100 µL Nafion solution (5%, DuPont, USA). After ultrasonication for 30 min, a homogeneous ink was obtained. A 21 µL liquid of the ink was dropped on the glassy carbon electrode head with a geometric area of 0.196 cm^2 and dried at 80 ^oC prior for the rotating disk electrode (RDE) testing. The preparation of the working electrode with 20 wt.% Pt/C as catalyst was similar to the above. The electrochemical measurements were performed using three-electrode system in 0.1 M KOH solution on the CHI 760E electrochemical workstation. A carbon rod and an Ag/AgCl electrode in saturated KCl solution were used as counter electrode and reference electrode, respectively. Before the ORR measurements, the cyclic voltammograms (CVs) were recorded at a sweep rate of 50 mV/s from -1.0 to 0.2 V (vs. Ag/AgCl) in N_2-saturated 0.1 M KOH solution to obtain a stable electrochemical profile. Next, the background current were got using the linear sweep voltammograms (LSVs) method at the same conditions. Then the currents at 400, 625, 900, 1225, 1600, 2025 rpm were got in O_2-saturated 0.1 M KOH solution and the ORR current curves was corrected for the background current. The OER currents were got using LSV method at a sweep rate of 5 mV/s from 0.2 to 1.0 V (vs. Ag/AgCl) in N_2-saturated 0.1 M KOH solution.

Results and discussion

Synthesis and Infrared Spectra

Complex **1** was synthesized by adding H_2MPCA, $CdCl_2{\cdot}2.5H_2O$ and imidazole in a molar ratio of 1:1:2 in EtOH-H_2O solution; complex **2** was synthesized by slow evaporation of acidizing DMF-MeOH-H_2O solution including H_2MPCA, NaOH and $CoCl_2{\cdot}6H_2O$ in a molar ratio of 2:2:1; and complex **3** was synthesized by adding H_2MPCA, $CdCl_2{\cdot}2.5H_2O$ and 2,2'-bpy in a molar ratio of 2:2:1 in DMF-MeOH-H_2O solution. Imidazole, NaOH, and 2,2'-bpy may play a role of base/template. IR spectra of complexes **1-3** are shown in Fig. S1. A strong and broad absorption peak around 3600-3000 cm^{-1} should be attributed to the stretching vibration of OH, indicating that all the complexes include H_2O molecule. The strong peaks at 1630 (for **1),** 1685 (for **2)**, and 1700 (for **3)** cm^{-1}, as well as 1436 (for **1)**, 1452 (for **2)** and 1461 (for **3)** cm^{-1}can be attributed to ν_{as} (OCO) and ν_s (OCO) stretching vibrations of the ligands. The strong peaks at 1530 (for **1)**, 1526 (for **2)** and 1518 (for **3)** cm^{-1}should be stretching vibrations of the C=N bond. The peaks at 744 (for **1**), 795 (for **2)** and 780 (for **3)** cm^{-1} are attributed to δ(OCO) bending vibrations of the ligands.[27] For **1**, there is no peak at 1680-1740 cm^{-1}, indicating that all carboxylic groups are deprotonated. These assignments are supported by the X-ray crystal structure analysis.

Crystal structures description of 1, 2 and 3

Single-crystal X-ray diffraction analysis showed that complex **1** crystallized in the triclinic space group *P*$\bar{1}$. The coordination sphere of Cd(II) ion is shown in Fig. 1, each Cd(II) ion employs six-coordination mode and coordinates with four oxygen atoms from four water molecules, and two nitrogen atoms from two $HMPCA^-$ anions, leading to the formation of an octahedral structure. In which, $N1^i$, O3, N1 and $O3^i$ locate at the equatorial plan positions and O3, $O3^i$ are at the axial direction. The bond angels of O-Cd1-N are in the range of 89.43 (16)˚ - 90.57 (16)˚, and that of O3-Cd1-$O3^i$, N1-Cd1-$N1^i$ and O4-Cd1-$O4^i$ are all 180˚, further indicating the geometries around each metal center are all octahedral. The bond distances of Cd1-N and Cd1-O are 2.298(4) Å, and in the range of 2.297(4)- 2.320(4) Å, respectively (Table S1), which are close to the values observed in other pyrazolecarboxylate based Cd(II) complexes.[27, 45] It is interesting that complex **1** is a zwitterionic complex; Fig. 1 clearly shows that carboxylic group

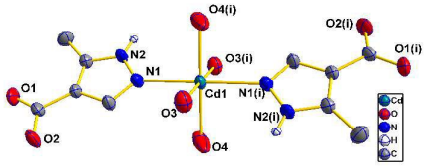

Fig. 1. The coordination environment of complex **1**. Symmetry code: (i) $-x, -y, -z$.

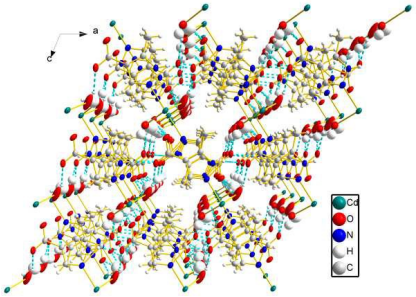

Fig. 2. 3D grid of complex **1**. (Dashed lines represent hydrogen bonds)

of H_2MPCA is deprotonated, but the carboxylate group does not coordinate with Cd(II) ion, only N atom does, resulting in $[Cd(HMPCA)_2(H_2O)_4]$ acquiring a zwitterionic nature.[46, 47] To our knowledge, it is the first zwitterionic complex containing $HMPCA^-$. The independent mononuclear components $[Cd(HMPCA)_2(H_2O)_4]$ are connected through intermolecular hydrogen bonds N(2)-H(2)---O(2), O(3)-H(3A)---O(1), O(3)-H(3B)---O(1) (Table S2) to form a 3D supramolecular network (Fig. 2).

Complex **2** crystallized in the monoclinic space group $P2_1/c$. As shown in Fig. 3, the coordination sphere of Co(II) ion is similar to that of Cd(II) ion in complex **1** except that two lattice H_2O molecules were replaced by two DMF molecules, and two $HMPCA^-$ anions replaced by two H_2MPCA molecules. In complex **2**, $[Co(H_2MPCA)_2(DMF)_2(H_2O)_2]^{2+}$ cations, which both

acted as hydrogen bond donors and acceptors, and Cl^- anions connected with each other via three kinds of hydrogen bonds (O-H---Cl, N-H---O, C-H---O) (Table S2) to form a 2D layer (Fig. 4). These 2D layers further pack a 3D supramolecular framework via intermolecular interaction (Fig. S2). The average bond distances of Co1-N and Co1-O are 2.126 and 2.093 Å respectively (Table S1), closing to the values observed in other Co(II) complexes.[26] Complex **3** features a unique 3D framework based on trinuclear $[Cd_3Cl_2(HMPCA)_4(H_2O)_2]$ secondary building units (SBUs). The coordination environment of Cd(II) ion is shown in Fig. 5a. Each Cd2(II) ion, adopting six-coordination mode, connects two N atoms and two O atoms from four different $HMPCA^-$ ligands, and two μ- Cl^- ions,

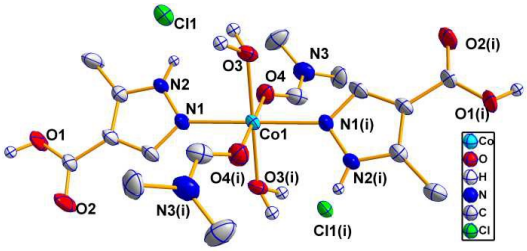

Fig. 3. The coordination environment of complex **2**. Symmetry code: (i) $-x+1, -y+1, -z+2$.

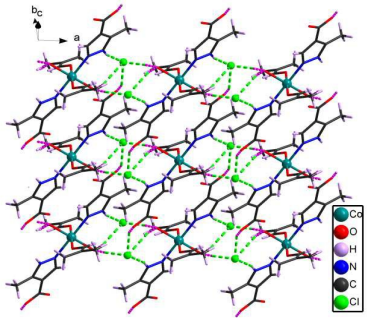

Fig. 4. 2D structure of complex **2**.

forming an octahedral geometry. In which, $N1^{iv}$, $N1^{v}$, $O3^{i}$, $O3^{iii}$ locate at the equatorial plane positions and Cl3, $Cl3^{ii}$ are at the apical positions. Cd1(II) ion is also six-coordinate, surrounded by one μ-Cl^- ion, one N atom from one $HMPCA^-$ ligand, one O atom from one coordinated water molecule, and three O atoms from two $HMPCA^-$ ligands, leading to a distorted octahedral geometry. Cd2 and two crystallographically equivalent Cd(II) ions ($Cd1^{ii}$, Cd1) form a trinuclear cluster structure via two chlorine bridges. These trinuclear clusters are further bridged to form a 3D framework containing channels along the *c* axis by two coordination modes of $HMPCA^-$ anions (see Scheme 1 and Fig. 5b).

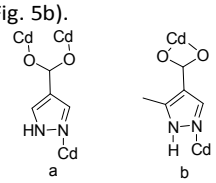

Scheme 1. Two coordination modes of $HMPCA^-$ anions in complex **3**.

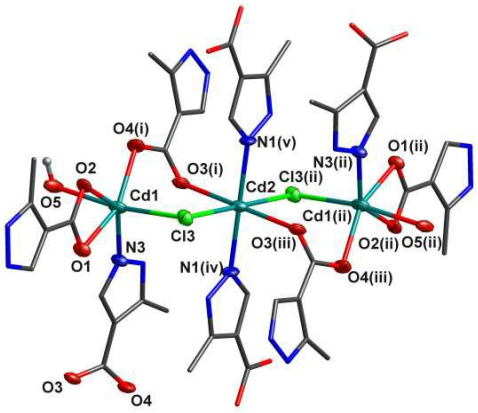

(a)

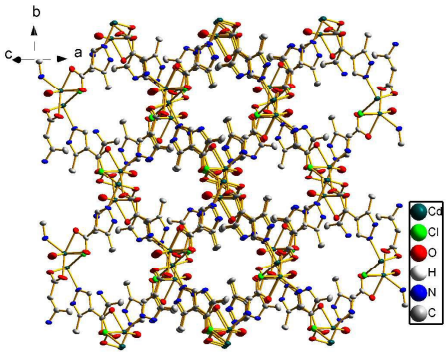

(b)

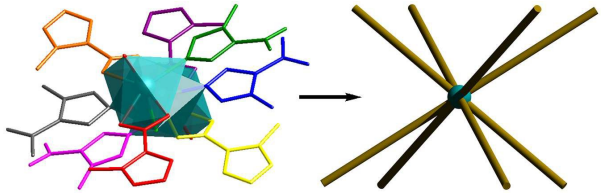

(c)

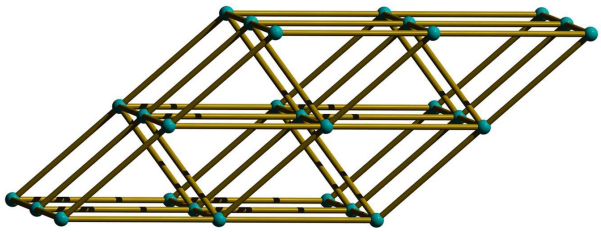

(d)

Fig. 5. View of complex **3:** (a) the coordination environment of Cd(II). Symmetry codes: (i) $-x+3/2, y+1/2, -z+3/2$; (ii) $-x+1, -y+1, -z+1$; (iii) $x-1/2, -y+1/2, z-1/2$; (iv) $x+1/2, -y+1/2, z-1/2$; (v) $-x+1/2, y+1/2, -z+3/2$. (b) 3D grid. (Free H_2O molecules and hydrogen bonds are removed). (c) The second building unit (SBU) composed of the Cd_3 trinuclear cluster bearing eight ligands,

and its simplified mode as an 8-connected node. (b) The 3D **bcu** framework constructed of Cd_3 trinuclear SBUs (highlighted in deep green balls).

The free H_2O molecules are clathrated in the channels via hydrogen bond interactions (O(5)-H(5A)---O(2), O(5)-H(5B)---O(6), O(6)-H(6A)---O(1) and O(6)-H(6B)---O(5)), while the stability of 3D structure is further increased by other hydrogen bonding interactions (N(2)-H(2) ---Cl(3) and C(5)-H(5C) ---O(6)) (see Fig. S3, and Table S2). PLATON calculation shows that the effective volume for the inclusion is about 256.1 $Å^3$ per unit cell, comprising 15.6% of the crystal volume of **3**. The average bond length of Cd-N, Cd-O and Cd-Cl are 2.288, 2.366 and 2.662 Å respectively, showing the atom coordination ability with Cd(II) ion is N>O>Cl.

The bond angles of N-Cd2-O, O-Cd1-Cl, and O-Cd1-O are in the range of 81.5 (2)- 95.5 (2)°, as listed in Table S1. From the perspective of topology, the trinuclear Cd(II) ions structural unit, connecting eight $HMPCA^-$ anions, should be considered as an 8-connected node (Fig. 5c). Therefore, the 3D framework of **3** belongs to a uninodal 8-connected body centered cubic (**bcu**) topological net with the Schläfli symbol of $(4^{24}\cdot6^4)$ (Fig. 5d).

Thermal Stability

In order to examine the thermal stabilities of complexes **1**-**3**, thermal gravimetric (TG) analyses were carried out from room temperature to 800 °C under nitrogen (Fig. S4). For **1**, a weight loss about 16.34 % from 105 °C to 191 °C, corresponds to four H_2O molecules loss (calcd 16.58 %), then a greater mass loss of 28.25 % from 191 °C to 302 °C maybe belong to the loss of one $HMPCA^-$ anion (calcd 28.78 %); above 302 °C, the residual substance decomposed gradually. For **2**, a weight loss about 32.63 % from 65 °C to 262 °C, corresponds to the loss of two DMF and two water molecules (calcd 32.25%); the mass loss of 33.92% from 262 °C to 403 °C may be attributed to the loss of one H_2MPCA and 2 Cl^- ions (calcd 35.08%); subsequently, the residual substance decomposed gradually, the pyrolysis product is CoO (calcd 13.27%, found 17.65%). For **3**, two H_2O molecules are lost between 63 °C to 250 °C (calcd 3.67%, found 3.55%); above 250 °C, the residual substance decomposed gradually.

Luminescent Properties

Luminescent complexes are currently of great interest because of their various applications in chemical sensors, photochemistry, and electroluminescent display.[48-50] Herein, the luminescent behaviors of ligand H_2MPCA, and complexes 1- 3 were investigated in the solid state at room temperature owing to the conjugate system of the ligand (Fig. 6 and Fig. S5). Upon excitation at 337 nm, the strongest emission peak for the ligand appears at 473 nm, corresponding to the n-π*/π-π*transitions.[14b] The emission peaks maxima are obsvered at 521 nm (λ_{ex} = 321 nm) in 1, 506 nm (λ_{ex} = 331 nm) in 2, and 521 nm (λ_{ex} = 320 nm) in 3. Compared with the ligand, the maximum emission wavelengths of complexes 1-3 all exhibit a red-shift, which may be caused by the variations of the highest occupied molecular orbital (HOMO) and lowest unoccupied molecular orbital (LUMO) energy levels after the ligand H_2MPCA coordinates to the metal ions.[50b]

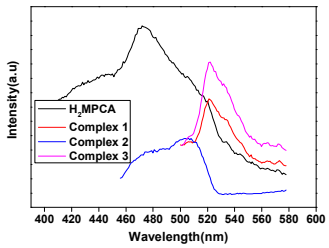

Fig. 6. Solid-state emission spectra of ligand H_2MPCA, complexes **1**, **2** and **3**

Electrocatalytic activity for ORR and OER of complex 2

The electrocatalytic activities of complex **2** for ORR and OER were investigated at the glassy carbon electrodes using the linear sweep voltammograms (LSVs). For comparison, the electrocatalytic activities of carbon black and 20 wt.% Pt/C were also tested. As shown in Fig. 7a, the ORR onset potentials (-0.11 V) of complex **2** is higher than -0.15 V of carbon black, but lower than 0.08 V of 20 wt.% Pt/C (Table 2). The variation trends of the half-wave potentials and the current densities at -0.3 V are same with that of the onset potentials for them (Table 2). These results indicate that the ORR activity of complex **2** is better than carbon black, and lower than 20 wt.% Pt/C. Cyclic voltammetry (CV) curves of the complex **2** modified electrode in a N_2- and O_2-saturated 0.1M KOH solution at a scan rate of 50 mV s^{-1} are displayed in Fig. S6 . From it, we can observe a strong cathodic reduction peak at −0.38 V (vs. Ag/AgCl electrode) in the O_2-saturated KOH solution, and a very weak cathodic reduction peak in the N_2-saturated solution. The result also indicates that the complex **2** has a pronounced catalytic activity for ORR. Fig. 7b shows the OER activities of complex 2, carbon black and 20 wt.% Pt/C. The current density at 0.9 V for complex **2** is 16.03 mA cm^{-2},

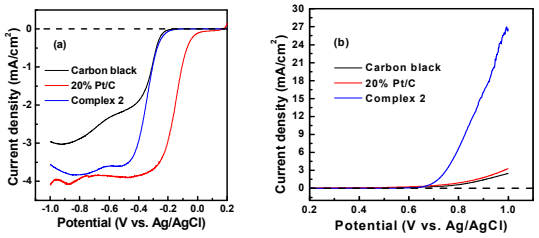

Fig. 7. LSVs of carbon black, 20 wt.% Pt/C, complex **2** samples: (a) ORR and (b) OER.

not only far higher than carbon black but also than 20 wt.% Pt/C (Table 2). This shows that the OER activity of complex **2** is far better than carbon black and 20 wt.% Pt/C. The comparison of the OER catalysts at 10 mA cm^{-2} is a commonly considered metric with relevance to solar fuel synthesis.[51] The complex **2** catalyst achieved a current density of 10 mA cm^{-2} at 1.808 V (vs. RHE, see Fig. S7), which corresponds to an overpotential of 578 mV.

Table 2. ORR and OER activities of samples at 1600 rpm.

Samples	Onset Potential (V)	Half-wave Potential (V)	Current Density at -0.3 V (mA cm^{-2})	Current Density at 0.9 V (mA cm^{-2})
Carbon black	-0.15	-0.34	-0.83	1.42
20 wt.% Pt/C	0.08	-0.15	-3.69	1.80
Complex **2**	-0.11	-0.23	-0.89	16.03

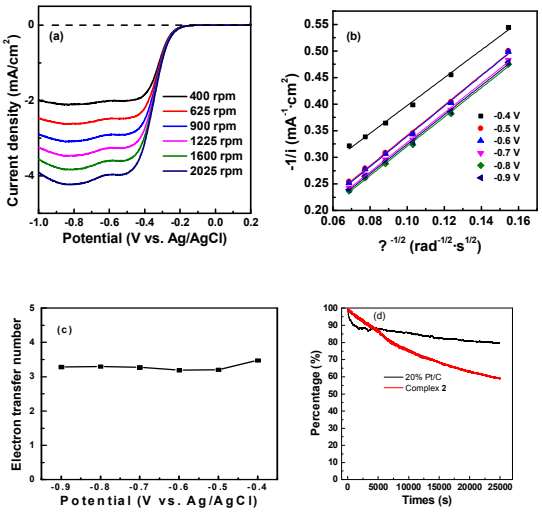

Fig. 8. RDE LSVs of (a) ORR at 400-2025 rpm in O_2-saturated 0.1 M KOH. (b) Koutecky-Levich polts of complex **2.** (c) Electron transfer number of complex **2**. (d) Chronoamperometric responses (percentage of current retained versus operation time) of complex **2** and Pt/C at a rotation rate of 1600 rpm and -0.3V in O_2-saturated 0.1MKOH electrolytes.

The overpotential value of complex **2** is higher than those of meso-Co_3O_4 catalyst (426 mV),[52] Co_3O_4/N-doped graphene,[34] Co_3O_4C-NA,[35] N-doped graphene-CoO[53] and IrO_2/C,[54] but comparable to that of Co_3O_4 nanocrystals/carbon nanotubes[55] (~550 mV at 10 mA cm^{-2} in 1.0 M KOH electrolyte) and mesoporous Co_3O_4[56] (Table S1), also demonstrating it has high catalytic activity for OER. The LSVs of complex **2** as electrocatalyst in RDE in 400~2025 rpm are showed in Fig. 8. The current density of ORR becomes bigger with the increasing of the rotational speed of RDE (Fig. 8a), this is because the rapid speed is benefit for the oxygen diffusion and transmission in electrolyte solution. The Koutecky-Levich polts of complex **2** are showed in Fig. 8b, indicating the Levich slopes are linear at the applied potentials. The number of the electron transfer (n) for each oxygen molecule in ORR was obtained by the Koutecky-Levich equation[57a] (see ESI). As can be seen in Fig. 8c, the number of the electron transfer is almost kept constant (average 3.37) from -0.4 ~ -0.9 V, which shows that the ORR catalyzed by complex **2** can occur via a 2- electron and 4-electron mixed process, but mainly via a 4-electron process.[57b] The rotating ring-disk electrode (RRDE) measurement (Fig. S8, see ESI) further proves that there is negligible ring current, and n, calculated from RRDE curves in the Fig. S9, is about 3.6-3.8 over the potential range from 0.15 to 0.7 V vs RHE, along with 7-20.8% H_2O_2 production. Both of the experimental results demonstrate that the four-electron process is the dominating pathway for the oxygen reduction on the complex **2** electrode, which will benefit the application of it as an electrocatalyst with high efficiency.[58] The long-term stability of complex **2** and 20 wt.% Pt/C for ORR were assessed by the chronoamperometric method (Fig. 8d). Although complex **2** exhibits a much faster decrease compared to 20 wt.% Pt/C, it still maintain about 60% of initial current density after 25.000 s of continuous operation. The OER stability test result of complex **2** is shown in Fig. S10 after cycling 1000 times, the OER activity of complex 2 at 0.9 V changed from 16.03 mA cm^{-2} to 3.65 mA cm^{-2}, corresponding to an activity loss of 77.2 %. Such larger activity loss may be related to the structure of complex **2** destroyed under the highly oxidizing conditions of durability test. This stability problem may be solved applying a complex containing variable valence metal ions (Co(II) ion et al) with high physicochemical stability. The related research is under way in our laboratory.

Conclusion

We successfully synthesized two mononuclear complexes $[Cd(HMPCA)_2(H_2O)_4]$ (**1**) and $[Co(H_2MPCA)_2(DMF)_2(H_2O)_2]Cl_2$ (**2**), and a 3D coordination polymer $[Cd_3Cl_2(HMPCA)_4(H_2O)_2]\cdot 2H_2O$ (**3**). In **1** and **2**, independent units are linked by intermolecular weak interactions to form 3D supramolecular frameworks. While in **3**, trinuclear Cd (II) ions clusters are bridged by $HMPCA^-$ anions with two coordination modes to form an 8-connected 3D network with channels. Complexes **1**-**3** all display green fluorescence in the solid state at room temperature. When complex **2** was applied as an electrocatalyst in alkaline solution, it exhibited excellent catalytic activity for OER, far exceeding 20 wt.% Pt/C catalyst, and certain catalytic activity for ORR. This work hence demonstrates a promising route to obtain no precious metal-based bi-functional catalysts for lithium–air batteries from transition metal complexes.

Acknowledgements

We thank the National Natural Science Foundation of China (No. 20671045, 20971060 and 21101018), the Natural Science Foundation of State Key Laboratory of Coordination Chemistry, the Project Funded by the Priority Academic Program Development of Jiangsu Higher Education Institutions for the financial support.

Notes and references

1 O. M. Yaghi, G. M. Li and H.Li, *Nature,* 1995, **378**, 703–704.

2 L. E. Kreno, K.Leong, O. K. Farha, M.Allendorf, R. P.Van Duyne and J. T.Hupp, *Chem. Rev.,* 2012, **112,** 1105–1125.
3 J-R. Li, J.Sculley and H-C. Zhou, *Chem. Rev.***.,** 2012, **112,** 869–932
4 (a)D.Uraguchi, Y.Ueki and T.Ooi, *Science,* 2009, **326,** 120–123. (b) D-W Tan, J-B. Xie, Q. Li, J-C. Li, H-X. Li, H-Y. Li and J-P. Lang, *Dalton Trans.*, 2014, **43**, 14061-14071.
5 M.X. Yao, Q. Zheng, X.M. Cai, Y.Z. Li, Y. Song and J.L. Zuo, *Inorg. Chem*., 2012, **51,** 2140–2149.
6 Z. Zhang, H.Yoshikawa and K. Awaga, *J. Am. Chem. Soc.,* 2014, **136,** 16112–16115.
7 M. Nagarathinam, K. Saravanan, E.J.H. Phua, M.V. Reddy, B.V.R. Chowdari and J.J.Vittal, *Angew. Chem*., 2012, **124***,* 5968–5972.
8 (a)Q. Liu, L.L.Yu, Y.Wang, Y.Z.Ji, J.Horvat, M.L.Cheng, X.Y.Jia and G.X.Wang, *Inorg. Chem*., 2013**, 52**, 2817–2822. (b) Q. Liu, X. Liu, C. Shi, Y. Zhang, X. Feng, M. L. Cheng, S. Su and J. Gu, *Dalton Trans.*, 2015, **44**, 19175-19184. (c) X. Liu, C. Shi, W. Zhai, M. L. Cheng, Q. Liu, and G. Wang, *ACS Appl. Mater. Interfaces,* 2016, **8,** 4585-4591. (d) C. Shi, Q. Xia, X. Xue, Q. Liu and H-J. Liu, *RSC Adv.*, 2016, **6**, 4442-4447.
9 B. L. Chen, L. B.Wang, Y. Q. Xiao, F. R.Fronczek, M.Xue, Y. J.Cui and G. D. Qian, *Angew. Chem. Int. Ed.,* 2009, **48**, 500–504.
10 P. Yang,M-S Wang, J-J. Shen, M-X Li, Z-X. Wang, M. Shao and X. He, *Dalton Trans.,* 2014, **43**, 1460–1470.
11 (a) Y. Gong, M. M. Zhang, W. Hua, J. L. Sun, H. F. Shi, P. G. Jiang, F. H. Liao and J. H. Lin, *Dalton Trans.,* 2014, **43**, 145–151. (b) J-B. Xie, J-J. Bao, H-X. Li, D-W Tan, H-Y. Li and J-P. Lang, *RSC Adv.*, 2014, **4**, 54007-54017.
12 X. H. Zhou, Y. H. Peng, X. D. Du, C. F. Wang, J. L. Zuo and X. Z.You, *Cryst. Growth Des.,* 2009, **9**, 1028–1035.
13 Y. Q. Sun, J. Zhang, Y. M. Chen and G. Y. Yang, *Angew. Chem. Int. Ed.,* 2005, **44**, 5814–5817.
14 (a)X. Feng, B. Liu, L. Y. Wang, J. S. Zhao, J. G. Wang, W. S. Ng and X. G. Shi, *Dalton Trans.,* 2010, **39**, 8038–8049. (b) Z-Q. Shi, Y-Z. Li, Z-J. Guo and H-G. Zheng, *CrystEngComm*, 2014, **16**, 900–909.
15 J. Xia, B. Zhao, H. S. Wang, W. Shi, Y. Ma, H. B. Song, P. Cheng, D. Z. Liao and S. P. Yan, *Inorg. Chem.,* 2007, **46**, 3450–3458.
16 C. Heering, I. Boldog, V. Vasylyeva, J. Sanchiz and C. Janiak, *CrystEngComm*, 2013, **15**, 9757–9768.
17 S. Su, Y. Zhang, M. Zhu, X. Song, S. Wang, S. Zhao, S. Song, X. Yang and H. Zhang, *Chem. Commun.,* 2012, **48**, 11118–11120.
18 C. Montoro, F. Linares, E. Q. Procopio, I. Senkovska, S. Kaskel, S. Galli, N. Masciocchi, E. Barea and J. A. R. Navarro, *J. Am. Chem. Soc.,* 2011, **133**, 11888–11891.
19 X. L. Qi, C. Zhang, B. Y.Wang, W.Xue, C. T. He, S. Y. Liu, W. X. Zhang and X. M. Chen, *CrystEngComm*, 2013, **15**, 9530–9536.
20 H. Liu, G. S. Yang, C. B. Liu, Y. Lin, Y. Yang and Y .Gong, *J. Coord. Chem.,* 2014, **67**, 572–587.
21 E. Q. Procopio, F. Linares, C.Montoro, V. Colombo, A.Maspero, E. Barea and J. A. R. Navarro, *Angew. Chem. Int. Ed.,* 2010, **49**, 7308–7311.
22 S.Wannapaiboon, M. Tu and R.A. Fischer, *Adv. Funct. Mater.,* 2014, **24**, 2696–2705.
23 J. Lincke, D.Lässig, M. Kobalz, J. Bergmann, M. Handke, J. Mollmer, M. Langer, C. Roth, A. Möller, R. Staudt and H. Krautscheid, *Inorg. Chem.,* 2012, **51**, 7579–7586.
24 C. Liu, Y. Gong, Y. Chen and H.Wen, *Inorg. Chim. Acta.,* 2012, **383**, 277–286.
25 25 L. Wang, F. Tao, M. Cheng, Q. Liu, W. Han, Y. Wu, D.Yang and L.Wang, *J. Coord. Chem.,* 2012**, 65,** 923–933.
26 J. Bao, M. Cheng, Q. Liu, W. Han, Y. Ji, C. Zhai, J. Hong and X. Sun, *Chinese J. Inorg.Chem.,* 2013, **29**, 1504–1512.
27 S. Su, M.-L. Cheng, Y. Ren, C. Zhai, F. Tao and Q. Liu, *Transition Met Chem.,* 2014, **39**, 559–566.
28 A. Kraytsberg and Y. Ein-Eli, *J. Power Sources,* 2011, **19**, 886–893.
29 K.Takechi, T. Shiga and T. Asaoka, *Chem. Commun.,* 2011, **47**, 3463–3465.
30 A.Débart, A.J. Paterson, J. Bao and P.G. Bruce, *Angew. Chem. Int. Ed.,* 2008, **47**, 4521–4524.
31 Y.-C. Lu, Z. Xu, H.A.Gasteiger, S. Chen, K. Hamad-Schifferli and Y. Shao-Horn, *J. Am. Chem. Soc.,* 2010, **132**, 12170–12171.
32 A. K. Thapa and T. Ishihara, *J. Power Sources*., 2011, **196**, 7016–7020.
33 K. L. Pickrahn, S.W. Park, Y. Gorlin, H.-B.-R. Lee, T. F. Jaramillo and S. F. Bent, *Adv. Energy Mater.,* 2012, **2***,* 1269–1277.
34 Y. Liang, Y. Li , H.Wang, J. Zhou, J.Wang, T. Regier and H. Dai , *Nat. Mater.,* 2011, **10** , 780-786.
35 T. Y. Ma, S. Dai, M. Jaroniec and S. Z. Qiao, *J. Am. Chem. Soc.,* 2014, **136**, 13925–13931.
36 L.Li, S-H. Cai, S. Dai and A. Manthiram, *Energy. Environ. Sci.,* 2014, **7**, 2630-2636.
37 W. M. Li, A. P.Yu, D. C. Higgins, B. G. Llanos and Z.W. Chen, *J. Am. Chem. Soc.,* 2010, **132**, 17056–17058.
38 T. Palaniselvam, H. B. Aiyappa and S. Kurungot, *J. Mater. Chem.,* 2012, **22**, 23799–23805.
39 R. Zhang, J. Ma, W. Wang, B. Wang and R. Li, *J. Electroanal.Chem.,* 2010, **643**, 31–38.
40 J. Mao, L. Yang, Ping. Yu, X. Wei and L. Mao, *Electrochem. Commun***.,** 2012**, 19***,* 29–31.
41 J M. ahan, Z. Liu and K. P. Loh, *Adv. Funct. Mater.,* 2013, **23**, 5363–5372.
42 J. Chen, H. Xi, X. Zhang, Q. Meng, Y. Jiang and X. Sun, *Fine Chemicals.,* 2007, **24,** 199–201.
43 G. M. Sheldrick, *SHELXTL-97, Program for X-ray Crystal Structure Determination*. University of Göttingen, Germany. 1997
44 V. D. Oleg, J. B. Luc and J. G.Richard, *J. Appl. Cryst*., 2009, **42**, 339–341.
45 L.Chen, F.Tao, L.Wang, J.Hong, X.Jia, J. Bao, Y-Z. Ji, M. Cheng and Q. Liu, *Z. Anorg. Allg. Chem.*, 2013, **639**, 552–557.
46 M.Kurmoo, C.Estournés, Y.Oka, H.Kumagai and K.Inoue, *Inorg. Chem*., 2005, **44**, 217 –224.
47 Y.Wu, L.Yu, M.Cheng, W.Han, L.Wang, X.Guo and Q.Liu, *Chin. J. Chem.,* 2012, **30**, 1045–1051.
48 Y. J.Cui, Y. F.Yue, G. D.Qian and B. L. Chen, *Chem. Rev.,* 2012, **112**, 1126–1162.
49 X-P. Zhang, V.Y. Chang, J.Liu, X-L.Yang, W.Huang, Y.Li, C-H.Li, G.Muller and X-Z.You, *Inorg. Chem.,* 2015**, 54**, 143–152.
50 (a) Z.Hu, B. J. Deibert and J.Li, *Chem. Soc. Rev.,* 2014, **43**, 5815–5840. (b) M. Li, Y-F. Peng, S. Zhao, B-L. Li and H-Y. Li, *RSC Adv.*, 2014, **4**, 14241-14247.
51 C. C. L. McCrory, S. Jung, J. C. Peters and T. F. Jaramillo, *J. Am. Chem. Soc.,* 2013, **135**, 16977–16987.
52 Y. J. Sa, K. Kwon, J.Y. Cheon, F. Kleitzc and S. H. Joo, *J. Mater. Chem. A*, 2013, **1**, 9992–10001
53 S. Mao, Z. Wen, T. Huang, Y. Hou, J. Chen, *Energy Environ. Sci.* 2014, **7,** 609–616.
54 Y. Zhao, R. Nakamura, K. Kamiya, S. Nakanishi, K. Has himoto, *Nat. Commun.* 2013, **4**, 2390.
55 J. Wu, Y. Xue, X. Yan, W. Yan, Q. Cheng and Y. Xie, *Nano Res.*, 2012, **5**, 521–530.
56 H. Tüysüz, Y. J. Hwang, S. B. Khan, A.M. Asiri and P. Yang, *Nano Res.*, 2013, **6**, 47–54.
57 (a) M. Jahan, Q. Bao and K.P. Loh, *J. Am. Chem. Soc.*, 2012, **134,** 6707–6713. (b)F. Yin, G. Li and H. Wang, *Catal. Commun.,* 2014, **54**, 17–21.
58 (a) S. Li, L. Zhang, H. Liu, M. Pan, L. Zan and J. Zhang, *Electrochim.Acta.* 2012, **55**, 4403-4411. (b) H. Yin, H. Tang, D. Wang, Y. Gao and Z. Tang, *ACS Nano*, 2012, **6,** 8288-8297.

Figure for the Table of Contents

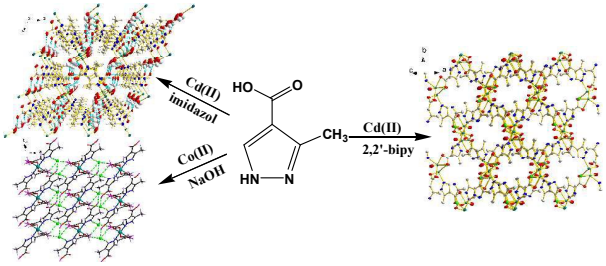

Mononuclear complexes $[Cd(HMPCA)_2(H_2O)_4]$ (**1**) and $[Co(H_2MPCA)_2(DMF)_2(H_2O)_2]Cl_2$ (**2**), and 3D coordination polymer $[Cd_3Cl_2(HMPCA)_4(H_2O)_2]\cdot 2H_2O$ (**3**) have been synthesized. As a bifunctional catalyst, complex **2** exhibited excellent catalytic activity for oxygen evolution reaction (OER) and certain catalytic activity for oxygen reduction reaction (ORR)